An Approach for Modelling the Structural Dynamics of a Mechanical System based on a Takagi-Sugeno Representation

Sebastian J. Pieczona[1], Fabio Muratore[1], Michael F. Zaeh[1]

[1]Institute for Machine Tools and Industrial Management (*iwb*)

Technische Universitaet Muenchen, Boltzmannstr. 15, 85748 Garching, Germany

Abstract

In order to design a controller or run a simulation, an appropriate mathematical model of an investigated system is necessary. Such a mathematical model is also utilized to describe the structural behavior of a mechanical system. Current methods to face the modelling challenges are limited to the description of predefined discrete points of a system. In order to model the mechanical behavior of an arbitrary point along a surface line or within a surface area, we propose an adaption of continuous Takagi-Sugeno Fuzzy Systems (TSFS) for structural mechanical systems. Consequently, the structural dynamics of specific points are modelled in a modal state space representation and utilized as subsystems of the fuzzy system. This approach leads to nonlinear differential equations containing the dynamics of all analyzed points and their interpolation. Thus, a continuous approximation of the properties between the discrete subsystems is possible, thereby outlining the main novelty of this concept. The proposed representation provides the advantages of an TSFS and is also applicable to fields such as model based controller design. The accuracy and performance of our approach is verified by an experimental setup and measurements of the system behavior in the time domain.

Keywords

Takagi-Sugeno Fuzzy System, computational intelligence, structural dynamics

1 INTRODUCTION

Today, models are used in nearly every discipline to characterize a system's specific behavior or its relations. An example taken from biology is the modeling of population dynamics [1]. Within the domain of industrial management, relational models are used to describe numerous influences affecting production [2]. In the field of machine tools, especially considering the cutting process, the knowledge of the structural behavior is of great importance. Such a model can be utilized e. g. for analyzing transient excitation responses or for defining an active vibration compensation controller [3]. The specification of a similar model, which characterizes the structural dynamics of a system using a predefined amount of discrete positions, is state of the art. A good overview regarding this topic is given by [4, 5]. To the best of the authors' knowledge, examination of the structural dynamics within a specified area of an object has not been investigated until now. For this purpose, we propose a method from computational intelligence (CI), an adapted Takagi-Sugeno fuzzy system (TSFS), to achive this goal.

In the past, CI has been applied to a wide range of research tasks in the domain of machine tools, e. g. control tasks [6, 7] or the description of machining processes [8]. An approach for modelling a mechnical system, which partly includes structural dynamics, was presented in [9, 10]. For this purpose, both approaches utilize TSFS. The first publication focuses on a universal specification of the model description. Therein, the authors take advantage of the inherent stability condition of quadratic Lyapunov functions, which analytically guarantees a correct system behavior. This approach is demonstrated using an inverted pendulum on cart as an application example. The second publication is devoted to modeling as well as to controller design. In contrast to [9], the object of investigation is a building. The presented methods were proven to allow a description of the nodal system behavior. The definition of a TSFS in modal representation has not been mentioned. This leads to a model that is capable of specifying the structural dynamics of discrete points. Compared to this, a fuzzy frequency response estimation from experimental data for mechanical structures of aircraft and aerospace vehicles is presented in [12]. The primary objective is to take uncertainties into account and to describe the system's boundaries in magnitude and phase of a bode plot. In the end, this new frequency response estimation can be used for control design and robust stability analysis.

In this paper the proposed TSFS contains the structural dynamics of predefined points and the area inbetween. For this purpose we take advantege of a modal representation, which leads to no changes in the state vector of the interpolated TSFS subsystems.

The remainder of the paper is organized as follows: Section 2 gives a short introduction to structural dynamics and fuzzy systems. In section 3, the novel modelling method is explained in detail. The performance of the proposed approach is confirmed in section 4 by experimental results.

2 FUNDAMENTALS

In this section the differential equations of a mechanical system, the modal state space representation of its structural dynamics and the basics of TSFS are recapitulated.

2.1 Equations of motion

Regarding a mechanical system with N degrees of freedom (dof) and proportional viscous damping the motion equation is as follows

$$\boldsymbol{M}\ddot{\boldsymbol{q}}(t) + \boldsymbol{D}\dot{\boldsymbol{q}}(t) + \boldsymbol{K}\boldsymbol{q}(t) = \boldsymbol{f}(t). \tag{1}$$

Therein, $\boldsymbol{q}(t) \in \mathbb{R}^{N \times 1}$ is the (nodal) displacement vector, $\boldsymbol{M} \in \mathbb{R}^{N \times N}$ is the mass matrix, $\boldsymbol{D} \in \mathbb{R}^{N \times N}$ is the damping matrix, $\boldsymbol{K} \in \mathbb{R}^{N \times N}$ is the stiffness matrix and $\boldsymbol{f}(t) \in \mathbb{R}^{N \times 1}$ is the external load vector. To shorten the notation the explicit formulation of time dependency will not be carried out in the following equations. According to [4] the matrices of the modal parameters natural frequency ω_r, damping ratio ζ_r and mass-normalized eigenvectors (mode shape vectors) $\boldsymbol{\phi}_r \in \mathbb{R}^{N \times 1}$ are defined as

$$\boldsymbol{\Omega} = \begin{bmatrix} \omega_1 & & 0 \\ & \ddots & \\ 0 & & \omega_n \end{bmatrix}, \tag{2a}$$

$$\boldsymbol{Z} = \begin{bmatrix} \zeta_1 & & 0 \\ & \ddots & \\ 0 & & \zeta_n \end{bmatrix} \text{ and} \tag{2b}$$

$$\boldsymbol{\Phi} = \begin{bmatrix} \phi_{1,1} & \cdots & \phi_{1,n} \\ \vdots & \cdots & \vdots \\ \phi_{N,1} & \cdots & \phi_{N,n} \end{bmatrix}. \tag{2c}$$

Thereby, it is $\boldsymbol{\Omega}, \boldsymbol{Z} \in \mathbb{R}^{n \times n}$ and $\boldsymbol{\Phi} \in \mathbb{R}^{N \times n}$ with $n \leq N$ as the number of observed modes. By using these parameter matrices subject to the criterions $2\boldsymbol{Z}\boldsymbol{\Omega} = \boldsymbol{\Phi}^{\mathrm{T}}\boldsymbol{D}\boldsymbol{\Phi}$, $\boldsymbol{I} = \boldsymbol{\Phi}^{\mathrm{T}}\boldsymbol{M}\boldsymbol{\Phi}$ as well as $\boldsymbol{\Omega}^2 = \boldsymbol{\Phi}^{\mathrm{T}}\boldsymbol{K}\boldsymbol{\Phi}$ and the modal coordinates $\boldsymbol{q}_m$, which satisfy the condition

$$\boldsymbol{q} = \boldsymbol{\Phi}\boldsymbol{q}_m \tag{3}$$

eq. (1) can be transformed into

$$\ddot{\boldsymbol{q}}_m + 2\boldsymbol{Z}\boldsymbol{\Omega}\dot{\boldsymbol{q}}_m + \boldsymbol{\Omega}^2\boldsymbol{q}_m = \boldsymbol{\Phi}^{\mathrm{T}}\boldsymbol{f}. \tag{4}$$

This differential equation characterizes the motion of a linear and proportionally viscously damped mechanical system with n modelled (structural) modes. Note, all modal variables are denoted by the index m.

2.2 Modal state space representation

The system described by eq. (4) can be written as the subsequent state space model

$$\ddot{\boldsymbol{q}}_m + 2\boldsymbol{Z}\boldsymbol{\Omega}\dot{\boldsymbol{q}}_m + \boldsymbol{\Omega}^2\boldsymbol{q}_m = \boldsymbol{\Phi}^{\mathrm{T}}\boldsymbol{B}\boldsymbol{u} = \boldsymbol{B}_m\boldsymbol{u}, \tag{5a}$$

$$\boldsymbol{y} = \boldsymbol{C}\boldsymbol{q} = \boldsymbol{C}_m\boldsymbol{q}_m, \tag{5b}$$

in which $\boldsymbol{B} \in \mathbb{R}^{N \times p}$, $\boldsymbol{u} \in \mathbb{R}^{p \times 1}$ and $\boldsymbol{B}_m \in \mathbb{R}^{n \times p}$ describe the p-dimensional input of the system. The q-dimensional system output is determined by $\boldsymbol{y} \in \mathbb{R}^{q \times 1}$, $\boldsymbol{C} \in \mathbb{R}^{q \times N}$ and $\boldsymbol{C}_m \in \mathbb{R}^{q \times n}$.

Considering a new coordinate vector

$$\begin{aligned} \boldsymbol{x} &= [\boldsymbol{x}_1^{\mathrm{T}} \quad \cdots \quad \boldsymbol{x}_n^{\mathrm{T}}]^{\mathrm{T}} \\ &= [q_{m,1} \quad \dot{q}_{m,1} \quad \cdots \quad q_{m,n} \quad \dot{q}_{m,n}]^{\mathrm{T}}, \end{aligned} \tag{6}$$

where $\boldsymbol{x}_r = [q_{m,r} \quad \dot{q}_{m,r}]^{\mathrm{T}} \in \mathbb{R}^{2 \times 1}$, with $r = 1, \ldots, n$, contains the modal displacement $q_{m,r}$ and the modal velocity $\dot{q}_{m,r}$. Similar to [5], this leads to the following modal state space representation for the rth mode:

$$\begin{aligned} \dot{\boldsymbol{x}}_r &= \begin{bmatrix} \dot{q}_{m,r} \\ \ddot{q}_{m,r} \end{bmatrix} = \begin{bmatrix} \dot{q}_{m,r} \\ \boldsymbol{b}_{\mathrm{m,r}}^{\mathrm{T}}\boldsymbol{u} - \omega_r^2 q_{m,r} - 2\zeta_r\omega_r\dot{q}_{m,r} \end{bmatrix} \\ &= \begin{bmatrix} 0 & 1 \\ -\omega_r^2 & -2\zeta_r\omega_r \end{bmatrix}\boldsymbol{x}_r + \begin{bmatrix} \boldsymbol{0}^{\mathrm{T}} \\ \boldsymbol{b}_{\mathrm{m,r}}^{\mathrm{T}} \end{bmatrix}\boldsymbol{u} \\ &= \boldsymbol{\mathcal{A}}_r\boldsymbol{x}_r + \boldsymbol{\mathcal{B}}_r\boldsymbol{u}, \end{aligned} \tag{7a}$$

$$\boldsymbol{y}_r = [\boldsymbol{c}_{m,r} \quad \boldsymbol{0}] = \boldsymbol{\mathcal{C}}_r\boldsymbol{x}_r, \tag{7b}$$

where $\boldsymbol{b}_{\mathrm{m,r}}^{\mathrm{T}} \in \mathbb{R}^{1 \times p}$ and $\boldsymbol{c}_{m,r} \in \mathbb{R}^{q \times 1}$ are the rth row of $\boldsymbol{B}_m$ and the rth column of $\boldsymbol{C}_m$, respectively. The dynamic matrix of the entire system $\boldsymbol{\mathcal{A}} \in \mathbb{R}^{2n \times 2n}$ is given by

$$\boldsymbol{\mathcal{A}} = \begin{bmatrix} \boldsymbol{\mathcal{A}}_1 & & \boldsymbol{0} \\ & \ddots & \\ \boldsymbol{0} & & \boldsymbol{\mathcal{A}}_n \end{bmatrix}. \tag{8}$$

Complementary, the input matrix $\boldsymbol{\mathcal{B}} \in \mathbb{R}^{2n \times p}$ and the output matrix $\boldsymbol{\mathcal{C}} \in \mathbb{R}^{q \times 2n}$ of the modal state space model are defined as

$$\boldsymbol{\mathcal{B}} = \begin{bmatrix} \boldsymbol{\mathcal{B}}_1 \\ \vdots \\ \boldsymbol{\mathcal{B}}_n \end{bmatrix} = \begin{bmatrix} \boldsymbol{0}^{\mathrm{T}} \\ \boldsymbol{b}_{\mathrm{m,1}}^{\mathrm{T}} \\ \vdots \\ \boldsymbol{0}^{\mathrm{T}} \\ \boldsymbol{b}_{\mathrm{m,n}}^{\mathrm{T}} \end{bmatrix}, \tag{9}$$

$$\boldsymbol{\mathcal{C}} = [\boldsymbol{\mathcal{C}}_1 \quad \cdots \quad \boldsymbol{\mathcal{C}}_n] = [\boldsymbol{c}_{m,1} \quad \boldsymbol{0} \quad \cdots \quad \boldsymbol{c}_{m,n} \quad \boldsymbol{0}]. \tag{10}$$

Finally, the eqs. (6) to (10) conclude in the ensuing linear time invariant (LTI) system

$$\dot{\boldsymbol{x}} = \boldsymbol{\mathcal{A}}\boldsymbol{x} + \boldsymbol{\mathcal{B}}\boldsymbol{u}, \tag{11a}$$

$$\boldsymbol{y} = \sum_{r=1}^{n} \boldsymbol{y}_r = \boldsymbol{\mathcal{C}}\boldsymbol{x}, \tag{11b}$$

which will be used in this study to describe the structural dynamics of mechanical systems.

2.3 Takagi-Sugeno modelling

Based on the definition of fuzzy sets in [11] and the description of fuzzy systems introduced in [13], a TSFS allows the description of a nonlinear system behavior as a combination of (local) linear systems. The included if-then rules of these TSFS consist of a premise part and a conclusion part. Within the first, the premise variables' degree of membership to the fuzzy sets of the rule is determined. In the second part, functional relationships are formulated, which are combined in a weighted sum. Thereby, the result of each rule is a weighted degree of activation.

Using a notation similar to [14], the ith model rule, with $i = 1, \ldots, R$, of a TSFS with linear consequent functions can be stated as

if $p_1 = F_{i,1}$ and ... and $p_L = F_{i,L}$,

then $\begin{cases} \dot{x} = \mathbf{A}_i x + \mathbf{B}_i u, \\ y = C_i x, \end{cases}$ (12)

where p_l, with $l = 1, \dots, L$, is the conceivably time-dependent premise variable and L denotes the number of premise variables. Furthermore $F_{i,l}$ is the fuzzy set corresponding to the lth premise variable of the ith rule and the local LTI system dynamic given by the matrices $\mathbf{A}_i, \mathbf{B}_i$ and C_i. According to [11] a fuzzy set F is characterized by a membership function $\mu(u)$, which associates each element u out of the universe of discourse U with a degree of membership in the interval $I = [0,1]$. The activation degree of the ith rule is defined as

$w_i(\boldsymbol{p}) = \prod_{l=1}^{L} \mu_{i,l}(p_l),$ (13)

where $\boldsymbol{p} = [p_1 \; \cdots \; p_L]$ is the collection of all premise variables, which are elements of U and $w_i(\boldsymbol{p}) \geq 0$ as well as $\sum_{i=1}^{R} w_i(\boldsymbol{p}) > 0$. In other words, the and-operator is implemented as the dot product. This leads to the normalized activation degree of the ith rule

$h_i(\boldsymbol{p}) = \frac{w_i(\boldsymbol{p})}{\sum_{j=1}^{R} w_j(\boldsymbol{p})},$ (14)

with $h_i(\boldsymbol{p}) \geq 0$ and $\sum_{i=1}^{R} h_i(\boldsymbol{p}) = 1$ due to the normalization. Building on these definitions, the dynamics are expressed as

$\dot{x} = \sum_{i=1}^{R} h_i(\boldsymbol{p}) (\mathbf{A}_i x + \mathbf{B}_i u),$ (15a)

$y = \sum_{i=1}^{R} h_i(\boldsymbol{p}) C_i x.$ (15b)

Generally, the result of this dynamic is nonlinear. It is called a blending of the linear subsystems, in which the weight of each subsystem h_i depends on the premise variables and the fuzzy sets' membership functions. The type of fuzzy reasoning by eqs. (13) to (15b) is named sum-prod inference.

3 TAKAGI-SUGENO BASED MODELLING OF STRUCTURAL DYNAMICS (TSSD)

The goal of this section is to create a TSFS, which is able to model the structural dynamics of a mechanical structure. First, a new matrix is introduced, to link the modal state space representation in eqs. (11a) to (11b) with the well-known receptance transfer function $\boldsymbol{\alpha}(\omega)$. Second, TSSD is developed by setting up an application-oriented TSFS similar to eq. (12) and defining two problem-specific membership functions.

3.1 Connection of notations

Taken form [5] the elements of the transfer function matrix for a proportionally viscously damped system equivalent to eq. (4) are stated as

$\alpha_{jk}(\omega) = \sum_{r=1}^{n} \frac{\phi_{jr}\phi_{kr}}{\omega_r^2 - \omega^2 + i2\zeta_r\omega_r\omega},$ (16)

where the indices j and k represent the measurement point and the driving point, respectively. Furthermore ϕ_{jr} denotes the jth

element of the mode shape vector $\boldsymbol{\phi}_r$ (rth column of $\boldsymbol{\phi}$ from eq. (2c)). In order to connect this definition with the state space model from section 2.2, eq. (16) is written as

$\alpha_{jk}(\omega) = \sum_{r=1}^{n} \frac{c_{m,jr} b_{m,rk}}{\omega_r^2 - \omega^2 + i2\zeta_r\omega_r\omega},$ (17)

with $c_{m,jr}$ and $b_{m,rk}$ being elements of the matrices $\mathbf{C}_m$ and $\mathbf{B}_m$, respectively. Note that the equality of eq. (16) and eq. (17) requires one constraint: All elements of the nodal system matrices $\mathbf{B}$ and $\mathbf{C}$, which describe the system's input and output, must be either 0 or 1. Following this constraint, the modal input and output matrices ($\mathbf{C}_m$ and $\mathbf{B}_m$), defined by eqs. (5a) and (5b), are composed of the elements from the mode shape matrix $\boldsymbol{\Phi}$.

Based on this relation we introduce the new matrix

$\boldsymbol{\Phi}_{ss} = \begin{bmatrix} \phi_{11} & 0 & \cdots & \phi_{1n} & 0 \\ 0 & \phi_{11} & \cdots & 0 & \phi_{1n} \\ \vdots & \vdots & \ddots & \vdots & \vdots \\ \phi_{N1} & 0 & \cdots & \phi_{Nn} & 0 \\ 0 & \phi_{N1} & \cdots & 0 & \phi_{Nn} \end{bmatrix},$ (18)

where ϕ_{ij}, with $i = 1, \dots, N$ and $j = 1, \dots, n$, are the entries of the eigenvector matrix $\boldsymbol{\Phi}$. Using $\boldsymbol{\Phi}_{ss} \in \mathbb{R}^{2N \times 2n}$ it is possible to calculate the modal state space model written in eqs. (11a) and (11b) directly from the nodal representation, which is more common. Therefore the subsequent equations

$\mathcal{B} = \boldsymbol{\Phi}_{ss}^{\mathrm{T}} \begin{bmatrix} \mathbf{0}^{\mathrm{T}} \\ b_1^{\mathrm{T}} \\ \vdots \\ \mathbf{0}^{\mathrm{T}} \\ b_n^{\mathrm{T}} \end{bmatrix}$ and (19)

$C = [c_1 \quad \mathbf{0} \quad \cdots \quad c_n \quad \mathbf{0}]\boldsymbol{\Phi}_{ss}$ (20)

show the link between the two representations.

3.2 Definition of TSSD

Relying on the presented theory in the previous sections we want to apply TSSD to a mechanical system described by the eqs. (5a) and (5b) as well as (11a) and (11b), respectively. Thereby, each pair of measurement and driving points is represented by one subsystem. This leads to the final TSSD representation in which the ith rule of the TSFS is stated as

if $\boldsymbol{p}_{in} = F_{i,in}$ and $\boldsymbol{p}_{out} = F_{i,out}$,

then $\begin{cases} \dot{x} = \mathcal{A}x + \mathcal{B}_i u, \\ y = C_i x, \end{cases}$ (21)

where $\boldsymbol{p}_{in}$, $\boldsymbol{p}_{out} \in \mathbb{R}^3$ are the premise variables of each rule and $F_{i,in}$ as well as $F_{i,out}$ are the fuzzy stets of the ith rule, describing the geometric area of the measurement and driving point.

This system operates in the following way: Prior to the application of the presented approach, the user determines a set of transfer functions at specific points on the test object's surface. Combined with the membership functions, these points shape the fuzzy sets $F_{i,in}$ and $F_{i,out}$ for all i. Depending on the

measurement and driving points, the premise variables have a specifiable degree of membership to all fuzzy sets. The final outcome is the displacement vector $\boldsymbol{y}$, which results from the weighted sum of all linear subsystems described by eq. (21). It is important to note, that in this eq. the dynamic matrix $\mathcal{A}$ is independent of the fuzzy rules. As a consequence, no state of $\boldsymbol{x}$ changes its physical sense, which is a fundamental requirement of a TSFS. Because of a possible blending between the subsystems an approximation between the analyzed points becomes available.

Since the transfer function is linear, switching the measurement and the driving point does not make a difference theoretically. Because of the utilization of a state space representation, every possible combination has to be taken into account to guarantee a fixed meaning of $\boldsymbol{x}$. As a conclusion, the number of rules for a fully described network is calculated as $\mathrm{R} = P^2$. Furthermore, P denotes the combined number of measurement and driving points, which have been determined by the user beforehand.

In the proposed approach, every fuzzy set is defined to have the same type of membership function, which has a significant influence on the final result. Before defining two function prototypes, we set up five requirements, which have to be fulfilled by every membership function:

1. The image region of a membership function covers the whole interval $I = [0, 1]$.

2. A membership function is continuous.

3. The core of each fuzzy set consists of exactly one unique element, which is determined by a measurement point or a driving point. This specific point in space is described by the vector $\boldsymbol{p}_{core,l} \in \mathbb{R}^3$, with $l = 1, \dots, P$. It is the only element of the fuzzy set F_l, whose degree of membership is equal to 1. Since $\boldsymbol{p}_{core,l}$ is specific for F_l, the intersection of two fuzzy sets' cores has to be the null set.

4. If the Euclidean distance between an examined point $\boldsymbol{p}_e \in \mathbb{R}^3$, i.e. one of the premise variables from eq. (21) and the core of an arbitrary fuzzy set $\boldsymbol{p}_{core,l} \in \mathbb{R}^3$, with $l = 1, \dots, P$, decreases monotonously, then the associated degree of membership has to increase monotonously.

5. For every element in the universe of discourse, i.e. for every point on the surface of the object, the sum of all degrees of membership is equal to 1. This can be regarded as a normalization, as mentioned in [14].

Due to the restrictions above a fuzzy set, e.g. F_l with $l = 1, \dots, P$, is characterized and named by its core element $\boldsymbol{p}_{core,l}$, which is equal to the vector $\boldsymbol{p}_l$ representing the specific point. If a measurement or driving point is used in multiple rules, then the associated fuzzy set, i.e. the membership function has to be identical. This is also true for the case that

a point is once used as a measurement point and another time as driving point. Therefore, the total number of points P is equal to the total number of fuzzy sets in the TSFS defined by eq. (21). The Euclidean distance between two points in space $\boldsymbol{p}_i$ and $\boldsymbol{p}_j$ is written as d_{ij} henceforth.

3.3 Membership function concepts

This section introduces two new concepts of membership function, which are supposed to fulfill the five aforementioned constraints. In addition to the definition, the function prototypes will be examined in a two-dimensional test environment.

3.3.1 Membership function concept 1

It is $\boldsymbol{p}_e \in \mathbb{R}^3$ the vector of the examined point, which can be any point on the object surface. The collection of all considered fuzzy sets is called termset of the linguistic variable $\mathcal{X}$ and denoted as $\boldsymbol{T}(\mathcal{X})$ [15]. Thereby, F_1 is the first of the P fuzzy sets and the last one is F_P. The membership function of the fuzzy set F_i, with $F_i, F_j, F_k \in \boldsymbol{T}(\mathcal{X})$, is defined as

$$\mu_i(\boldsymbol{p}_e) = \frac{\prod_{F_j = F_1, F_j \neq F_i}^{F_P} d_{ej}}{\sum_{F_k = F_1}^{F_P} \left(\prod_{F_j = F_1, F_j \neq F_k}^{F_P} d_{ej} \right)}. \tag{22}$$

Expressed in words, the eq. (22) states: The degree of membership of the point $\boldsymbol{p}_e$ to the fuzzy set F_i, defined by the point $\boldsymbol{p}_i$, is calculated by a ratio of distances in space. In eq. (22) the numerator holds the product of the distances from the examined point to all other points, which characterize the considered fuzzy sets. The denominator uses the same calculation rule for all fuzzy sets in $\boldsymbol{T}(\mathcal{X})$ and sums up the results.

3.3.2 Membership function concept 2

Under the same conditions as mentioned in the previous subsection, the membership function of the fuzzy set F_i is defined as

$$\mu_i(\boldsymbol{p}_e) = \begin{cases} \dfrac{1 - \dfrac{d_{ei}}{\hat{d}_i}}{\sum_{F_j = F_1}^{F_P} 1 - \dfrac{d_{ej}}{\hat{d}_j}} & \text{for } d_{ei} \leq \hat{d}_i, \\ 0 & \text{for } d_{ei} > \hat{d}_i. \end{cases} \tag{23}$$

with the parameter $\hat{d}_i$ defining a distance where the point i has an influence on the approximation of the examined point. Thus, this function prototype generates a seemingly piecewise linear relation between the distance and the degree of membership. However, due to the dependency of the Euclidean distances from $\boldsymbol{p}_e$ to the core elements of the fuzzy sets, which change simultaneously, the membership function in eq. (23) is nonlinear. In each case the distance of the examined point to one of the fuzzy set's core elements equals or exceeds the associated distance parameter, the slope of $\mu_i(\boldsymbol{p}_e)$ decreases.

Both of the introduced function prototypes fulfill all of the previously listed conditions and lead to nonlinear functions, that return the value 1 if $\boldsymbol{p}_e = \boldsymbol{p}_i$ and the

value 0 if $\boldsymbol{p}_e = \boldsymbol{p}_j$ with $j = 1, ..., P$ and $j \neq i$. The fifth requirement implies the benefit, by implementing this TSFS in software using one state-space system.

3.3.3 Test of the membership function concepts

Consider a not further specified arbitrary triangle in space, illustrated in figure 1. The points A, B and C mark the vertices, whereas M is the circumcenter. Because of this fact it is $d_{AM} = d_{BM} = d_{CM}$. Furthermore $\boldsymbol{r}$ indicates the direction in which a point T moves from M to A over the normalized time τ with a constant velocity. Therefore, this scenario yields a strong relationship between the normalized time and the distanced between the point T and the vertices. There exist three fuzzy sets F_A, F_B and F_C defined by their core elements $\boldsymbol{p}_A$, $\boldsymbol{p}_B$ and $\boldsymbol{p}_C$ as well as their membership functions $\mu_A(\boldsymbol{p}_T)$, $\mu_B(\boldsymbol{p}_T)$ and $\mu_C(\boldsymbol{p}_T)$, which depend on the test case.
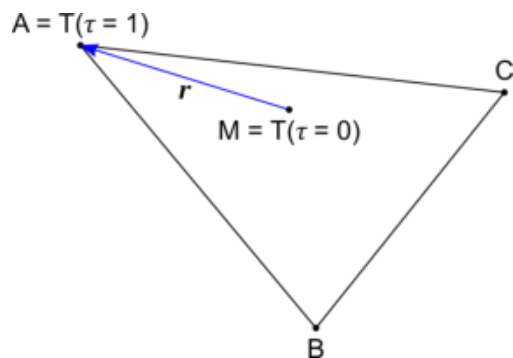
Figure 1 – Test environment for function prototypes

Due to the chosen setup the degree of membership from $\boldsymbol{p}_T$ to all fuzzy stets at $\tau = 0$ is $\frac{1}{3}$. In analogy to that the degree of membership at $\tau = 1$ is 1 for F_A as well as 0 for F_B and F_C. The two subsequent figures visualize the behavior of the different function prototypes from subsection 3.3.1 and 3.3.2, respectively.
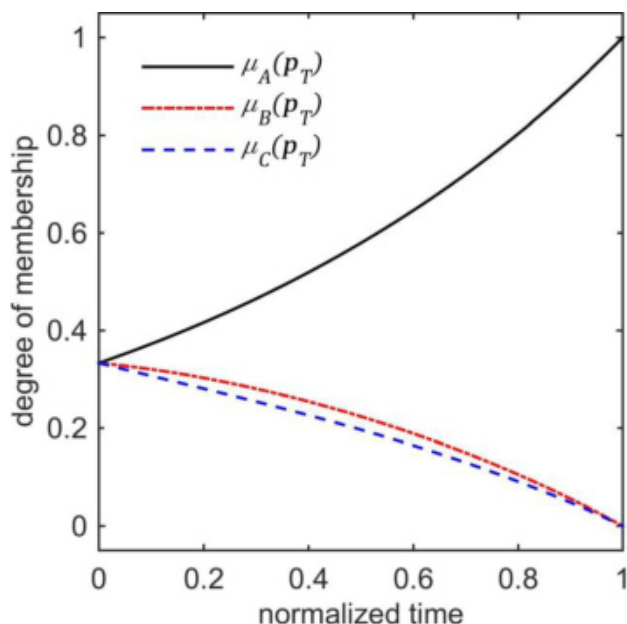
Figure 2 – Membership function concept 1
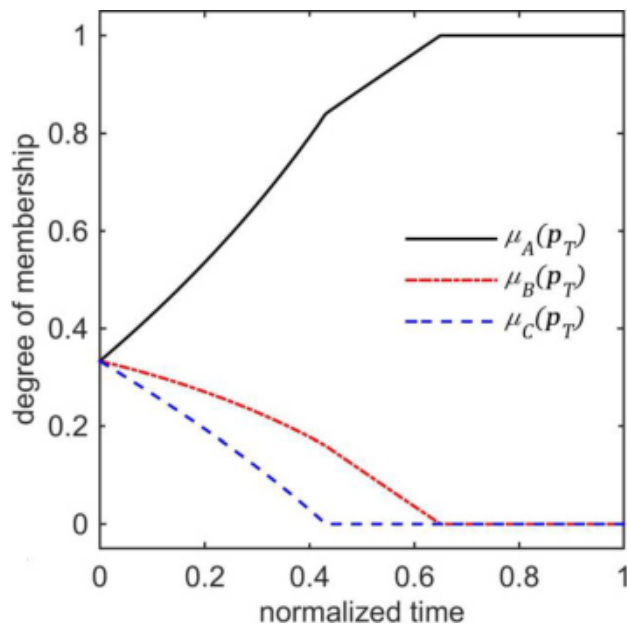
Figure 3 – Membership function concept 2

The figures 2 and 3 illustrate, that the two concepts of membership function fulfill all mentioned requirements. In case of the second concept, the distance parameters for all the fuzzy sets have been chosen equally as well as larger than the initial distance from the circumcenter and smaller than each side of the triangle. This determines the time in figure 3 at which $\mu_B(\boldsymbol{p}_T)$ and $\mu_C(\boldsymbol{p}_T)$ become zero. As mentioned beforehand, both function prototypes show a nonlinear characteristic.

4 APPLICATION OF TSSD

The validation of this approach was done by evaluating a series of measurements, which were carried out on an approximately two-dimensional steel plate mounted on four steel springs at the edges of the plate. The measurement points were arranged in a triangular grid shown by figure 4. Each side of the equilateral triangle is 100 mm. The points B, C, D and F mark the midpoint of the related lines. The driving point O (also measured) was located at the position $\boldsymbol{p}_O = [10\,\mathrm{mm} \quad 10\,\mathrm{mm} \quad 0\,\mathrm{mm}]^\mathrm{T}$ and the measurement point A was placed at $\boldsymbol{p}_A = [100\,\mathrm{mm} \quad 100\,\mathrm{mm} \quad 0\,\mathrm{mm}]^\mathrm{T}$ in relation to the global coordinate system. Note, that the positions of the points on the test surface as well as the relative positions of these points were chosen arbitrarly.
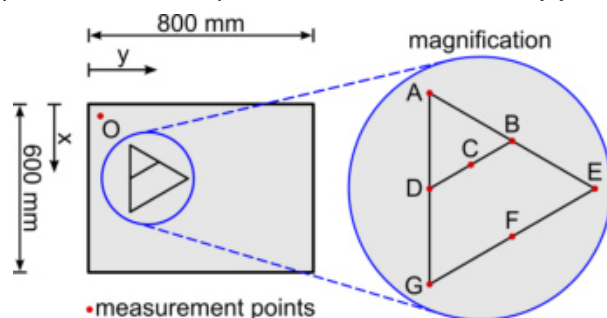
Figure 4 – Sketch of the steel plate (top view)

The goal was to show the performance of TSSD by comparing the measured system response of a specific point (here C) to the results computed by the TSFS in eq. (21) and the measured system response of the nearest point. The defined TSSD contains the dynamics of all illustrated points in figure 4, except C, resulting in 49 rules. As a measure for similarity the root mean square (RMS) was used. Considering two discrete signals $y_{des}[k]$ and $y[k]$ with K samples, the RMS of their difference $y_{diff}[k] = y_{des}[k] - y[k]$ is calculated as

$$RMS(y_{diff}[k]) = \sqrt{\frac{1}{K}\sum_{k=1}^{K} y_{diff}^2[k]}. \qquad (24)$$

This is a nonlinear measure, where big deviations have a disproportionately high impact.

Concerning the simulation, the inputs of all subsystems are the same recorded force excitation values provided by an impulse hammer. The outputs of the systems were calculated based on the modal parameters, which have been extraced beforhand. The results of the different TSFSs will be compared to three reference systems. They were chosen because of their minor deviation from the desired system behavior. Moreover the measurement points of the reference systems are the three closest to the measurement point of the target system. The approximation results of the transfer function from $\boldsymbol{p}_O$ to $\boldsymbol{p}_C$ are summarized in table 1. The contained index describes the output point, whereby y_{c1} and y_{c2} represent the results for TSSD using both membership function concepts from section 3.3. For each signal the driving point was O, hence it does not show up in the notation of the signals. This example of application represents a special case, because the described theory allows a continuous and erratic shifting of measurement and driving point. The last two columns of the table contain the RMS values of the deviation from each system's output to the true output y_C, in which lower numbers represent a better approximation. The evaluation includes the examination of two different time intervals. The point in time $t = 15\,s$ is of interest, because the amplitude is down to less then $50\,\%$ of the initial peak value. At $t = 150\,s$, the amplitude has decreased to less then $2\,\%$ of the initial peak value. These two statements apply to all signals.

signal	parameter	$RMS(y_C - y_i)\ [10^{-6}\ \text{m}]$	
		$t_{end} = 15\,\text{s}$	$t_{end} = 150\,\text{s}$
y_A	–	13.73	4.686
y_B	–	13.77	5.463
y_D	–	15.46	6.172
y_{c1}	–	10.47	4.093
y_{c2}	$\hat{d}_C = 51\,\text{mm}$	10.77	4.426
y_{c2}	$\hat{d}_C = 101\,\text{mm}$	10.21	3.948
y_{c2}	$\hat{d}_C = 151\,\text{mm}$	10.27	3.974

Table 1 – Comparison of the RMS values

Table 1 shows that both concepts of membership functions (outputs y_{c1} and y_{c2}) perform better than all three reference systems (outputs y_A, y_B and y_D). For better readability, the best result of TSSD and the reference systems have been highlighted for each time interval. In contrast to the first membership function prototype, the second is adjustable by the distance parameter $\hat{d}_C$. Increasing this parameter leads to a consideration of more subsystems, i.e. to a larger number of rules. Once $\hat{d}_C$ exceeds the largest appearing distance between the examined point and one of the measurement points ($d_{CG} = d_{CF}$), the effect is a change of the subsystems' weighting. As a result of the experiments it revealed that the optimal value of the distance parameter $\hat{d}_i$ varies for each target system.
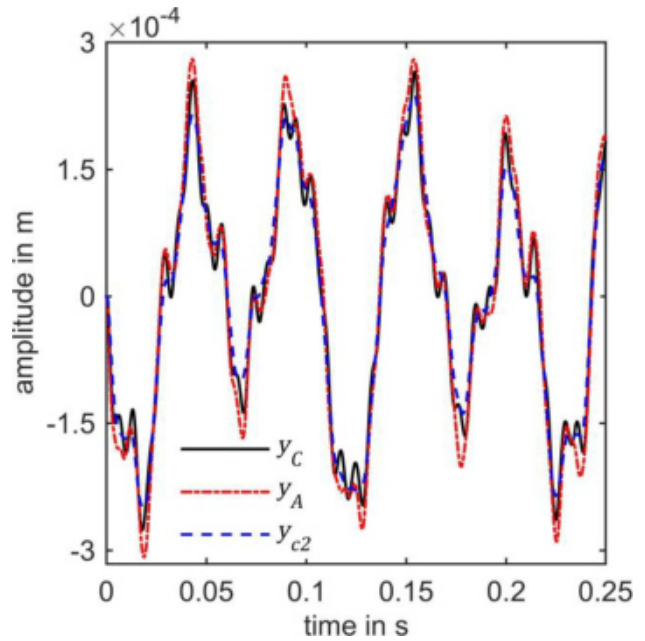
Figure 5 – Comparison of signals (time frame 1)
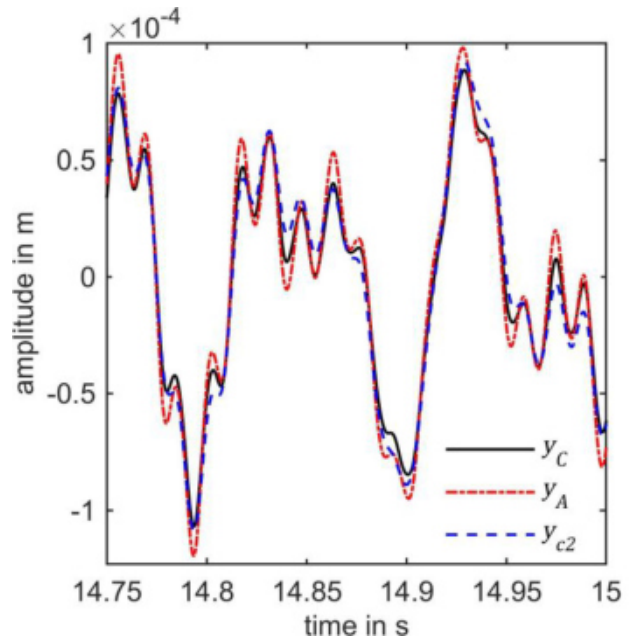
Figure 6 – Comparison of signals (time frame 2)

Furthermore, the figures 5 and 6 visualize the comparison of the best implementation of TSSD, i. e. the one from table 1 with the least RMS value (output y_{c2} with $\hat{d}_C = 101\,\text{mm}$) and the best reference system (output y_A) derived from the extracted modal parameters with respect to the desired system (output y_C). Figure 5 shows the time response of the three systems immediately after the hammer impact and figure 6 illustrates the behavior after $14.75\,\text{s}$. Both plots visualize and confirm the results in table 1. Although the TSSD output y_{c2} does not match the desired signal y_C perfectly, it states a better approximation than the nearest point results y_A, reducing the RMS error by about 26 % for the short time interval and by about 16 % for the long time interval.

5 CONCLUSIONS

Within this contribution a novel approach on the modelling of structural dynamics has been presented. The proposed method requires predefined points and their dynamic behavior in modal representation, which shape the required subsystems. In order to allow a blending between the subsystems a Takagi Sugeno fuzzy system has been utilized. This allows an approximation of the dynamics between the analyzed points, providing the behavior of not explicitly examined areas of the test object. The regulation of this interpolation is user-defined. To secure a correct implementation five requirements for the interpolation were specified. Furthermore, we presented two possible realization options and benchmarked them by an experimental setup. The results show the potential of the proposed approach and validate the introduced theory.

6 ACKNOWLEDGMENTS

7 REFERENCES

[1] Begon, M., Harper, J.L., Townsend, C.R., 1996, Ecology: Individuals, populations and communities, 3rd ed., Blackwell Science, Oxford.

[2] Plehn, C., Koch, J., Diepold, K., Stahl, B., Lohman. B., Reinhart, G., Zaeh, M.F., 2015, Modeling and Analyzing Dynamic Cycle Networks for Manufacturing Planning, Procedia CIRP, vol. 28: 149–154.

[3] Baur, M., Zaeh, M.F., 2012, Development and Experimental Validation of an Active Vibration Control System for a Portal Milling Machine, Proceedings of the 9th International Conference on High Speed Machining, vol. 9: 256–261.

[4] Ewins, D.J., 1995, Modal testing: Theory and practice, Research Studies Press, Taunton.

[5] Gawronski, W.K., 2004, Advanced structural dynamics and active control of structures, Springer-Verlag, New York.

[6] Ndzabukelwayo, S. M., Mpofu, K., Tlale, N., 2012, An intelligent fuzzy PID controller for a reconfigurable machine tool, International Conference on Information Security and Intelligence Control, 99–102.

[7] Huang, H., Li, A., Xu, L., 2008, Fuzzy control of milling process with constraint of spindle power, 7th World Congress on Intelligent Control and Automation, vol. 7: 7936–7939.

[8] Aguero, E., Alique, J.R., Haber, R., Rodriguez, C., 1993, Fuzzy modelling of machine-tool cutting process, Third International Conference on Industrial Fuzzy Control and Intelligent Systems, 191–196.

[9] Chen, C.-W., 2006, Stability conditions of fuzzy systems and its application to structural and mechanical systems, Advances in engineering software, vol. 37: 624–629.

[10] Chen, C.-W., Yeh, K., Chiang, W.-L., Chen, C.-Y., Wu, D.-J., 2007, Modeling, H∞ Control and Stability Analysis for Structural Systems Using Takagi-Sugeno Fuzzy Model, Journal of vibration and control, vol. 13: 1519–1534.

[11] Zadeh L.A., 1965, Fuzzy Sets, Information and control, vol. 8: 338–353.

[12] Ferreira, C.C.T., Luiz de Oliveira Serra, G., 2011, Fuzzy frequency response estimation from experimental data: Definition and application in mechanical structures of aircraft and aerospace vehicles, 9th IEEE International Conference on Control and Automation, vol 9: 1225–1230.

[13] Takagi, T., Sugeno, M., 1985, Fuzzy identification of systems and its applications to modelling and control, IEEE Transactions on Systems, Man, and Cybernetics, vol. 15: 116–132.

[14] Tanaka, K., Wang, H.O., 2001, Fuzzy Control Systems Design and Analysis: A Linear Matrix Inequality Approach, Wiley, New York.

[15] Zadeh, L.A., 1975, The Concept of a Linguistic Variable and its Application to Approximate Reasoning - I, Information sciences, vol. 8: 199–249.

8   BIOGRAPHY

Sebastian J. Pieczona was born in 1987 in Katowice (Poland) and received the Dipl.-Ing. degree in mechatronics from Technische Universitaet Muenchen (TUM) in 2012. He is currently a research associate at the *iwb* and is interested in research on control of galvanometer laserscanners.

Michael F. Zaeh was born in 1963 in Coburg (Germany). Since 2002 he is professor for machine tools and manufacturing technology (*iwb*) at Technische Universitaet Muenchen (TUM). He received the Dipl.-Ing. degree and the Dr.-Ing. degree in 1989 and 1993, respectively. From 1996 until 2002 he worked in the machine tool industry.
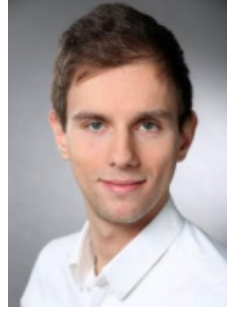
Fabio Muratore was born in 1989 in Bergisch-Gladbach (Germany) and received his B.Sc. degree at Technische Universitaet Muenchen (TUM) in 2013. Currently he is achieving his M.Sc. degree at TUM. During his studies he focused on control theory and computational intelligence.